*Inorg. Chem.* **2007**, *46*, 660–669


# Spin Coupling in the Supramolecular Structure of a New Tetra(Quinoline–TEMPO)Yttrium(III) Complex

**Luca Maretti,[†] Marilena Ferbinteanu,*[,‡,#] Fanica Cimpoesu,[‡,⊥] Saiful S. M. Islam,[†] Yasunori Ohba,[†,§] Takashi Kajiwara,[‡,§] Masahiro Yamashita,[‡,§] and Seigo Yamauchi*[,†]**

*Institute for Chemical Reaction Science, Tohoku University, Aoba-ku, Katahira 2-1-1, Sendai 980-8577, Japan, Department of Chemistry, Graduate School of Science, Tohoku University, Aramaki, Aoba-ku, Sendai 980-8578, Japan, and CREST, JST, Japan*

Received June 16, 2006

The newly synthesized tetra(quinoline–TEMPO)yttrium(III) potassium salt shows interesting structural features at the molecular and supramolecular levels, revealed by the analysis of the X-ray diffraction data. The magnetic susceptibility and EPR data corroborated with structural considerations showed that the exchange and dipolar spin coupling interactions are taking place at the nodes assembling the supramolecular 2D structure. The Y(III) center shows antiprismatic octacoordination, close to the idealized $D_2$ symmetry. The diamagnetic transition metal plays no role in mediating the radical interactions since the TEMPO-type fragments are remote from the chelating moieties of the ligand. In turn, significant interaction occurs on the nodes consisting in the quasi-rectangular coordination of potassium counterions by the spin-bearing TEMPO groups coming from four distinct complex units. The antiferromagnetic susceptibility was consistently modeled by a spin Hamiltonian based on the rectangle topology of four spins $S = {}^1/_2$. The fitted exchange parameters are $J_a = -5.1$ cm$^{-1}$ and $J_b = -3.4$ cm$^{-1}$ for the edges, imposing $J_d = 0$ for the diagonal. These values are in excellent agreement with the ab initio results $J_a = -4.83$ cm$^{-1}$, $J_b = -3.44$ cm$^{-1}$, $J_d = -0.07$ cm$^{-1}$ obtained in a CASSCF(12,8) calculation. Based on the reliability of the ab initio results we were able to select the presented $J$ parameters among several versions of multiple solutions with acceptable goodness of the fit. A methodological caveat about the artifacts of the automatic use of best fit parameters, in the absence of supplementary criteria, in the context of relative blindness of magnetic susceptibility modeling, is raised. The details of the EPR spectrum at 10 K are also consistent, in the frame of dipolar approximation, with the model of four interacting spins at the nodes of the supramolecular assembling.

## Introduction

The molecular magnetism of the systems involving radicals[1,2] is a fascinating field of research, complementary to the realm of magnetochemistry and material science exclusively based on metal ion compounds. The ferromagnetic phase transitions in the organic crystals of nitroxide radicals,[3] as well the nature of ferro[4] versus antiferro coupling[5] among related congeners, have attracted great attention. Complete understanding still represents a challenge since such phenomena are driven by genuine supramolecular effects.[6,7]

In order to fully comprehend the radical interaction phenomena at hand, a variety of advanced techniques, like

* To whom correspondence should be addressed. E-mail: yamauchi@tagen.tohoku.ac.jp (S.Y.), marilena@agnus.chem.tohoku.ac.jp (M.F.).
† Institute for Chemical Reaction Science.
‡ Department of Chemistry.
§ CREST.
# M.F. permanent address: University of Bucharest, Faculty of Chemistry, Department of Inorganic Chemistry Dumbrava Rosie 23, Bucharest 70254, Romania.
⊥ F.C. permanent address: Institute of Physical Chemistry, Splaiul Independentei 202, Bucharest 77208, Romania.

(1) (a) Kahn, O. *Molecular Magnetism*; VCH: Weinheim, Germany, 1993. (b) Benelli, C.; Gatteschi, D. *Chem. Rev.* **2002**, *102*, 2369−2388.
(2) Bencini, A.; Gatteschi, D. *EPR of Exchange Coupled Sytems*; Springer-Verlag: Berlin, 1990.
(3) (a) Chiarelli, R.; Novak, M. A.; Rassat, A.; Tholence, J. L. *Nature* **1993**, *363*, 147−149. (b) Takahashi, M.; Turek, P.; Nakazawa, Y.; Tamura, M.; Nozawa, K.; Shiomi, D.; Ishikawa, M.; Kinoshita, M. *Phys. Rev. Lett.* **1991**, *67*, 746−748.
(4) Pontillon, Y.; Grand, A.; Ishida, T.; Lelievre-Berna, E.; Nogami, T.; Ressouche, E.; Schweizer, J. *J. Mater. Chem.* **2000**, *10*, 1539−1546.
(5) (a) Duffy, W., Jr.; Dubach, J. F.; Pianetta, P. A.; Deck, J. F.; Strandburg, D. L.; Miedena, A. R. *J. Chem. Phys.* **1972**, *56*, 2555−2561. (b) Watanabe, I.; Wada, N.; Yano, H.; Okuno, T.; Awaga, K.; Ohira, S.; Nishiyama, K.; Nagamine, K. *Phys. Rev. B* **1998**, *58*, 2438−2441. (c) Ishida, T.; Ohira, S.; Ise, T.; Nakayama, K.; Watanabe, I.; Nogami, T.; Nagamine, K. *Chem. Phys. Lett.* **2001**, *330*, 110−117.



10.1021/ic0610841 CCC: $37.00 
Published on Web 12/30/2006

polarized neutron diffraction,[8] muon spin rotation,[9] combined with theoretical analyses have been used for detection and understanding of the interaction pathways.[10] Electron paramagnetic resonance (EPR) spectroscopy has also proven to be a powerful tool in the elucidation of interradical effects.[11] Furthermore, synthesis of new molecular systems comprising new topologies of interacting radicals is an important source in fundamental understanding. This promotes also the development of new spectroscopic methodologies.

Radical complexes of transition[12−14] and lanthanide metal ions[2,15] form a distinguished domain of study. In this area of research, various chemical and structural problems are encountered. These are ranging from subtle effects of radical interactions via ionic lanthanide centers,[16,17] up to the special effects such as the bistability due to semiquinone−catecholate valence tautomerism[18] in quinone-type ligands or in the lattice of donor−acceptor TCNQ alike systems.[19] A distinguished phenomenon is the lattice spin transition in certain nitroxide complexes,[20] a rather inedited case of spin crossover. Recently, a single-chain magnet based on nitronyl nitroxide ligand was discovered.[21]

Supramolecular pathways of interaction are usually observed when bulk magnetism, cooperativity, and hysteresis of magnetic properties are detected.[6a,22] In the radical systems, at the supramolecular scale, hydrogen bonding is often conceived as a parameter to control magnetic properties.[23]

The potential use in the material science of magnets and superconductors is one of the main corollaries of the interest devoted to radical systems chemistry.[24] Among other applications one may note that the nitroxide stable free radicals have been used as spin labels in biological systems,[25] as excited states quenchers,[26,27] or as radical coupling agents in "living" free radical polymerization,[28,29] and for spin catalysis in various oxidation processes.[30] Even probably yet a far goal, merely a desideratum, a possible application of the matrix-isolated interradical interactions is the qubit effect and quantum computing.[31]

Radical-type coordination chemistry mainly uses nitroxide-based ligands because of their relatively good stability.


(6) (a) Aoki, C.; Ishida, T.; Nogami, T. *Inorg. Chem.* **2003**, *42*, 7616−7625. (b) Hicks, R. G.; Lemaire, M. T.; Ohrstrom, L.; Richardson, J. F.; Thompson, L. K.; Xu, Z. Q. *J. Am. Chem. Soc.* **2001**, *123*, 7154−7159. (c) Papoutsakis, D.; Kirby, J. B.; Jackson, J. E.; Nocera, D. G. *Chem. Eur. J.* **1999**, *5*, 1474−1480.

(7) (a) Caneschi, A.; Gatteschi, D.; Rey, P. *Inorg. Chem.* **1991**, *30*, 3936−3941. (b) Iwamura, H.; Inoue, K.; Koga, N.; Hayamizu, T. In *Magnetism: A Supramolecular Function*; Kahn, O., Ed.; Kluwer: Dordrecht, The Netherlands, 1996; pp 157. (c) Kahn, O. *Acc. Chem. Res.* **2000**, *33*, 647−657.

(8) Pontillon, Y.; Caneschi, A.; Gatteschi, D.; Grand, A.; Ressouche, E.; Sessoli, R.; Schweizer, J. *Chem. Eur. J.* **1999**, *5*, 3616−3624.

(9) (a) Jeong, J.; Briere, T. M.; Sahoo, N.; Ohira, S.; Nishiyama, K.; Nagamine, K.; Das, T. P. *Phys. Rev. B* **2002**, *66*, 132411−132414. (b) Gatteschi, D.; Carretta, P.; Lascialfari, A. *Physica B* **2000**, *289−290*, 94−105.

(10) Briere, T. M.; Jeong, J.; Das, T. P.; Ohira, S.; Nagamine, K. *Physica B* **2000**, *289−290*, 128−131.

(11) (a) Martin, R. E.; Pannier, M.; Diederich, F.; Gramlich, V.; Hubrich, M.; Spiess, H. W. *Angew. Chem., Int. Ed.* **1998**, *37*, 2833−2840. (b) Shin, Y. K.; Levinthal, C.; Levinthal, F.; Hubbel, W. L. *Science* **1993**, *259*, 960−963.

(12) (a) Bencini, A.; Benelli, C.; Gatteschi, D.; Zanchini, C. *J. Am. Chem. Soc.* **1984**, *106*, 5813−5818. (b) Benelli, C.; Gatteschi, D.; Carnegie,D. W., Jr.; Carlin, R. L. *J. Am. Chem. Soc.* **1985**, *107*, 2560−2561.

(13) Ishii, N.; Ishida, T.; Nogami, T. *Inorg. Chem.* **2006**, *45*, 3837−3839.

(14) (a) Caneschi, A.; Gatteschi, D.; Lalioti, N.; Sessoli, R.; Sorace, L.; Tangoulis, V.; Vindigni, A. *Chem. Eur. J.* **2002**, *8*, 286−292. (b) Caneschi, A.; Gatteschi, D.; Lalioti, N.; Sangregorio, C.; Sessoli, R.; Venturi, G.; Vindigni, A.; Rettori, A.; Pini, M. G.; Novak, M. A. *Angew. Chem., Int. Ed.* **2001**, *40*, 1760−1763. (c) Carrasco, R.; Cano, J.; Ottenwaelder, X.; Aukauloo, A.; Journaux, Y.; Ruiz-Garcia, R. *Dalton Trans.* **2005**, 2527−2538.

(15) (a) Benelli, C.; Caneschi, A.; Gatteschi, D.; Laugier, J.; Rey, P. *Angew. Chem. Int. Ed. Engl.* **1987**, *26*, 913−915. (b) Caneschi, A.; Dei, A.; Gatteschi, D.; Poussereau, S.; Sorace, L. *Dalton Trans*. **2004**, 1048−1055. (c) Benelli, C.; Caneschi, A.; Gatteschi, D.; Sessoli, R. *Adv. Mater*. **1992**, *4*, 504−505. (d) Bussiere, G.; Beaulac, R.; Belisle, H.; Lescop, C.; Luneau, D.; Rey, P.; Reber, C. *Top. Curr. Chem.* **2004**, *241*, 97−118.

(16) (a) Tsukuda, T.; Ogita, M.; Suzuki, T.; Kaizaki, S. *Eur. J. Inorg. Chem.* **2004**, *22*, 4463−4469. (b) Lescop, C.; Bussiere, G.; Beaulac, R.; Belisle, H.; Belorizky, E.; Rey, P.; Reber, C.; Luneau, D. *J. Phys. Chem. Solids* **2004**, *65*, 773−779.

(17) (a) Benelli, C.; Caneschi, A.; Gatteschi, D.; Pardi, L. *Inorg. Chem.* **1992**, *31*, 741−746. (b) Sutter, J.-P.; Kahn, M. L.; Golhen, S.; Ouahab, L.; Kahn, O. *Chem. Eur. J.* **1998**, *4*, 571−576. (c) Sutter, J.-P.; Kahn, M. L.; Kahn, O. *Adv. Mater*. **1999**, *11*, 863−865. (d) Dei, A.; Gatteschi, D.; Massa, C. A.; Pardi, L.; Poussereau, S.; Sorace, L. *Chem. Eur. J.* **2000**, *6*, 4580−4586.

(18) (a) Pierpont, C. G. *Coord. Chem. Rev.* **2001**, *95*, 216−217. (b) Speier, G.; Tyeklár, Z.; Tóth, P.; Speier, E.; Tisza, S.; Rockenbauer, A.; Whalen, A. M.; Alkire, N.; Pierpont, C. G. *Inorg. Chem.* **2001**, *40*, 5653−5659. (c) Bachler, V.; Olbrich, G.; Neese, F.; Wieghardt, K. *Inorg. Chem.* **2002**, *41*, 4179−4193. (d) Ohtsu, H.; Tanaka, K. *Chem. Eur. J.* **2005**, *11*, 3420−3426.

(19) Manriquez, J. M.; Yee, G. T.; McLean, R. S.; Epstein, A. J.; Miller, J. S. *Science* **1991**, *252*, 1415−1417.

(20) Rey, P.; Ovcharenko, V. I. In *Magnetism: Molecules to Materials IV*; Miller, J. S., Drillon, M., Eds.; Wiley-VCH: Weinheim, Germany, 2002; pp 41−63 and references therein.

(21) (a) Bogani, L.; Sangregorio, C.; Sessoli, R.; Gatteschi, D. *Angew. Chem., Int. Ed.* **2005**, *44*, 5817−5821. (b) Bernot, K.; Bogani, L.; Caneschi, A.; Gatteschi, D.; Sessoli, R. *J. Am. Chem. Soc*. **2006**, *128*, 7947−7956.

(22) Hicks, R. G.; Lemaire, M. T.; Öhrström, L.; Richardson, J. F.; Thompson, L. K.; Xu, Z. *J. Am. Chem. Soc.* **2001**, *123*, 7154−7159.

(23) (a) Maruta, G.; Takeda, S.; Imachi, R.; Ishida, T.; Nogami, T.; Yamaguchi, K. *J. Am. Chem. Soc.* **1999**, *121*, 424−431. (b) Deumal, M.; Cirujeda, J.; Veciana, J.; Novoa, J. J. *Chem. Eur. J.* **1999**, *5*, 1631−1642. (c) Pontillon, Y.; Akita, T.; Grand, A.; Kobayashi, K.; Lelievre-Berna, E.; Pecaut, J.; Ressouche, E.; Schweizer, J. *J. Am. Chem. Soc.* **1999**, *121*, 10126−10133. (d) Akita, T.; Mazaki, Y.; Kobayashi, K. *J. Chem. Soc., Chem. Commun.* **1995**, 1861−1862.

(24) (a) Miller, J. S. *Angew. Chem., Int. Ed. Engl*. **1994**, *33*, 385−415. (b) Miller, J. S. *Adv. Mater.* **1992**, *4*, 435−438.

(25) (a) Arora, A.; Williamson, I. M.; Lee, A. G.; Marsh, D. *Biochemistry* **2003**, *42* (17), 5151−5158. (b) Sartori, E.; Toffoletti, A.; Corvaja, C.; Moroder, L.; Formaggio, F.; Toniolo, C. *Chem. Phys. Lett.* **2004**, *385*, 362−367. (c) Wright, P. J.; English, A. M. *J. Am. Chem. Soc.* **2003**, *125*, 8655−8665.

(26) Green, S. A.; Simpson, D. J.; Zhou, G.; Ho, P. S.; Blough, N. V. *J. Am. Chem. Soc.* **1990**, *112*, 7337−7346.

(27) (a) Blough, N. V.; Simpson, D. J. *J. Am. Chem. Soc.* **1987**, *110*, 1915−1917. (b) Kobori, Y.; Mitsui, M.; Kawai, A.; Obi, K. *Chem. Phys. Lett.* **1996**, *252*, 355−361. (c) Jockusch, S.; Liu, Z.; Ottaviani, F.; Turro, N. J. *J. Phys. Chem. B* **2001**, *105*, 7477−7481. (d) Mitsui, M.; Kobori, Y.; Kawai, A.; Obi, K. *J. Phys. Chem. A* **2004**, *108*, 524−531.

(28) (a) Hawker, C. J.; Bosman, A. W.; Harth, E. *Chem. Rev*. **2001**, *101*, 3661−3688. (b) Kamigaito, M.; Ando, T.; Sawamoto, M. *Chem. Rev*. **2001**, *101*, 3689−3746. (c) Knoop, C. A.; Studer, A. *J. Am. Chem. Soc*. **2003**, *125*, 16327−16333. (d) Ballesteros, O. G.; Maretti, L.; Sastre, R.; Scaiano, J. C. *Macromolecules* **2001**, *34*, 6184−6187. (e) Georges, M. K.; Lukkarila, J. L.; Szkurhan, A. R. *Macromolecules* **2004**, *37*, 1297−1303.

(29) Skene, W. G.; Scaiano, J. C.; Yap, G. P. A. *Macromolecules* **2000**, *33*, 3536−3542.

(30) (a) Semmelhack, F. M.; Schmid, C. R.; Cortés, D. A.; Chou, C. S. *J. Am. Chem. Soc.* **1984**, *106*, 3374. (b) Bolm, C.; Magnus, A. S.; Hilderbrand, J. P. *Org. Lett.* **2000**, *2*, 1173−1175. (c) De Luca, L.; Giacomelli, G.; Porcheddu, A. *Org. Lett.* **2001**, *3*, 3041−3043. (d) Ansari, I. A.; Gree, R. *Org. Lett.* **2002**, *9*, 1507−1509.

Several kinds of ligands are reported in the literature, and two modes of complexation are taken in consideration: (a) one with the direct interaction between the nitroxide and the metal[32,33] and (b) one where a pendent chelating part of the molecule coordinates the metal, thus separating the radical from the metal magnetic orbital.[34]

As an extension of our previous concern with radical ligands[28,35] and related complexes,[36] here we present the synthesis and study of the magnetic properties of a new tetra-[4-(3-hydroxy-2-methyl-4-quinolinoyloxy)-2,2,6,6-tetramethylpiperidine-1-oxyl] yttrium(III), potassium salt ($K^+[Y(QT)_4]^-$). The enolic moiety of the ligand affords chelating of four QTs to the yttrium center. The potassium counterion ensures the charge balance in the molecular unit and also plays a role in the supramolecular assembling. The coordination of TEMPO fragments to the potassium builds a two-dimensional (2D) structure and enables magnetic interactions via ionic bridges.

To the best of our knowledge this is the first example where the chelating appendix of a radical ligand and the radical itself participate in assembling the supramolecular structure. Not much information is available about similar cases since coordination of nitroxide to alkaline metal ions is restricted to one report.[37] The use of a diamagnetic central ion affords a better understanding of radical−radical spin effects.[38] These preliminary nitroxide/yttrium complex studies are to set the stage for further systematic investigations involving the substitution of yttrium(III) ion with paramagnetic lanthanides. The ab initio calculations, a proven useful complement to the phenomenological magneto−structural analysis,[39] were employed in this work also, as a rationalization tool.

## Experimental Section

**General.** All reagents and solvents were obtained from Wako Chemicals and used as received. The radical ligand 4-(3-hydroxy-2-methyl-4-quinolinoyloxy)-2,2,6,6-tetramethylpiperidine-1-oxyl free radical was prepared according to a procedure already reported.[35a]

**Synthesis.** One-half gram of 4-(3-hydroxy-2-methyl-4-quinolinoyloxy)-2,2,6,6-tetramethylpiperidine-1-oxyl free radical (QT) (1.4 mmol) was dissolved in 200 mL of 2-propanol, and 157 mg of potassium *t*-butoxide (1.4 mmol) was added. After 10 min 134 mg of $Y(NO_3)_3 \cdot 6H_2O$ (0.35 mmol) was added to the solution, and immediately a white precipitate of $KNO_3$ was formed. After 1 h the solution was filtered, and the solvent evaporated. The orange solid was then dissolved in 3 mL of acetonitrile, and after 1 day large orange-red crystals were obtained. IR (KBr, $cm^{-1}$) : 2977.6 (m), 2939 (m), 1645 (s), 1604.5 (m), 1544.7 (w), 1469.5 (s), 1361.5 (m), 1332.6 (s), 1313.3 (s), 1299.8 (s), 1247.7 (w), 1207.2 (s), 1151.3 (s), 1116.6 (w), 1085.7 (w), 1043.3 (w), 1018.2 (m), 1000.9 (m), 983.5 (m), 968.1 (w), 943 (w), 927.6 (w), 894.8 (w), 869.7 (w), 806.1 (m), 769.5 (m), 750.2 (m), 711.6 (w), 680.7 (w), 644.1 (w), 626.7 (w), 565 (w), 482.1 (m), 451.3 (w). Elemental analysis calcd (%) for $C_{80}H_{96}N_8O_{16}K$ (crystals were dried under vacuum): C, 61.84; H, 6.23; N, 7.21. Found: C, 61.67; H, 6.43; N, 7.30.

**Magnetic Susceptibility.** Variable-temperature magnetic susceptibility measurements was made using a SQUID magnetometer MPMS 5S (Quantum Design) at 1 T. Diamagnetic correction was determined from Pascal's constants.

**Electron Paramagnetic Resonance.** A continuous wave EPR spectrum was obtained on a JEOL JES-FE-2XG spectrometer. Temperature was controlled by an Oxford ESR 900 helium gas-flow system. The polycrystalline sample was dispersed in a small amount of Nujol and placed at the bottom of a 5 mm EPR tube, giving a randomly oriented system.

**Crystallographic Data Collection and Refinement of the Structure.** Data for the compound were collected by a Bruker SMART APEX diffractometer employing graphite-monochromated Mo K$\alpha$ radiation ($\lambda = 0.71073$ Å) at low temperature (200 K). The data integration and reduction were undertaken with SAINT and XPREP.[40] An empirical correction determined with SADABS[41] was applied to each data. The structure was solved by the direct method using SHELXS-97[42] and refined using least-squares methods on $F^2$ with SHELXL-97. Non-hydrogen atoms were modeled with anisotropic displacement parameters, and hydrogen atoms were placed by the differential Fourier syntheses and refined isotropically.

## Results and Discussion

**Molecular Unit and Supramolecular Assembling.** Yttrium(III) was selected as the central ion for its high coordination number abilities and stereochemical versatility (due to the missing factors of electron count versus ligand field stabilization in the $d^0$ configuration). The stereochemical factors are also enabling the pendent arm of the ligands to self-organize by intermolecular forces. The QT bears a chelating group similar to the enolic form of 2,4-pentanedione, which can be activated by a suitable base such as potassium *t*-butoxide. The diamagnetic properties of Y(III) are affording the resolution of intermolecular radical−radical coupling effects. The complex is formed in solution, by the metathesis of the potassium salt of the ligand, K(QT), and yttrium(III) nitrate, being followed by the immediate precipitation of the $KNO_3$ side product, completed by the slow crystallization of the complex.


(31) (a) Knight, P. *Science* **2000**, *287*, 441−442. (b) Di Vincenzo, D. P. *J. Appl. Phys.* **1997**, *81*, 4602. (c) Bennett, C. H.; Di Vincenzo, D. P. *Nature* **2000**, *404*, 247−255. (d) Prinz, G. A. *Science* **1998**, *282*, 1660−1663.

(32) Dickman, M. H.; Porter, L. C.; Doedens, R. J. *Inorg. Chem.* **1986**, *25*, 2595−2599.

(33) Porter, L. C.; Doedens, R. J. *Inorg. Chem.* **1985**, *24*, 1006−1010.

(34) Grand, A.; Rey, P.; Subra, R. *Inorg. Chem.* **1983**, *22*, 391−394.

(35) (a) Aspee, A.; Garcia, O.; Maretti, L.; Sastre, R.; Scaiano, J. C. *Macromolecules* **2003**, *36*, 3550−3556. (b) Ricci, A.; Chretien, M. N.; Maretti, L.; Scaiano, J. C. *Photochem. Photobiol. Sci.* **2003**, *2*, 487−492. (c) Aspee, A.; Maretti, L.; Scaiano, J. C. *Photochem. Photobiol. Sci.* **2003**, *2*, 1125−1129.

(36) Maretti, L.; Islam, S. S. M.; Ohba, Y.; Kajiwara, T.; Yamauchi, S. *Inorg. Chem.* **2005**, *44*, 9125−9127.

(37) Forbes, G. C.; Kennedy, A. R.; Mulvey, R. E.; Rodger, P. J. A. *Chem. Commun.* **2001**, 1400−1401.

(38) Pontillon, Y.; Bencini, A.; Caneschi, A.; Dei, A.; Gatteschi, D.; Gillon, B.; Sangregorio, C.; Stride, J.; Totti, F. *Angew. Chem., Int. Ed.* **2000**, *39*, 1786−1788.

(39) Bencini, A.; Dei, A.; Sangregorio, C.; Totti, F.; Vaz, M. G. F. *Inorg. Chem.* **2003**, *42*, 8065−8071.

(40) *SMART*, *SAINT*, and *XPREP*, area detector control and data integration and reduction software; Bruker Analytical X-ray Instruments Inc.: Madison, WI, 1995.

(41) Sheldrick, G. M. *SADABS*, empirical absorption correction program for area detector data; University of Göttingen: Göttingen, Germany, 1996.

(42) Sheldrick, G. M. *SHELX97*, *Programs for Crystal Structure Analysis*; University of Göttingen: Göttingen, Germany, 1998.

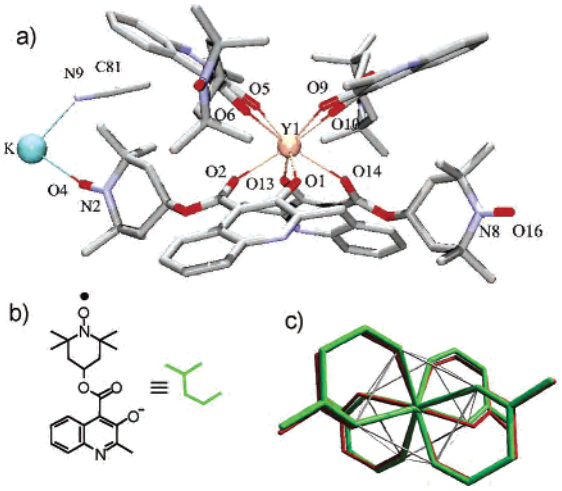


**Figure 1.** Structure of the $[Y(QT)_4]^-$ complex unit: (a) the asymmetric unit; (b) the constituent ligand; (c) the superposition between experimental coordination skeleton (green, front sticks) and the $D_2$ idealization (red stick overlapping behind).

The $K^+[Y(QT)_4]^-$ complex unit shows no rigorous symmetry element. However, it is worth observing its relative closeness to the $D_2$ symmetry and the square antiprism placement of the oxygen donor atoms of the bidentate ligands. The molecular unit and the ligand are shown in Figure 1, parts a and b, respectively.

Figure 1c illustrates, as close-up detail, the structural and symmetry aspects of the complex unit, representing the superposition between the experimental geometry and the $D_2$ idealized one. The green sticks (visible as front lines in Figure 1c) represent the experimental structure skeleton. It superposes well over the $D_2$ idealized one (drawn in red). At the end of the pendent arm of the ligands, proportional to the increased radius with respect to the center, the symmetry deviation becomes larger.

The idealization was obtained taking one ligand of the experimental structure, replicating it according to the operations of the $D_2$ group, and fitting correspondingly its local placement and orientation in order to achieve the optimal global match.

At the supramolecular scale, four $[Y(QT)_4]^-$ complex units are bridged by one potassium counterion through nitroxide-type coordination. Four TEMPO radicals from four distinct complex units are coordinated to a potassium ion. A two-dimensional architecture is obtained, as represented in Figure 2a. The potassium ion is also coordinating an acetonitrile molecule at the upper vertex of a flat pyramid. The acetonitrile molecule is slightly bent with respect to the apical axis. The structure of the self-organizing node, $\{(CH_3CN)K^+(QT)_4\}$, is shown in Figure 2b. Its idealized model, having $C_{2v}$ symmetry and the QT replaced by TEMPOL, is used for the following theoretical analyses and shown in Figure 2c.

The basic crystal parameters are shown in Table 1, and the illustrative bond lengths and angles are collected in Table 2. Due to the chemical asymmetry of the donors, the Y−O bond lengths are slightly different inside the chelating rings.

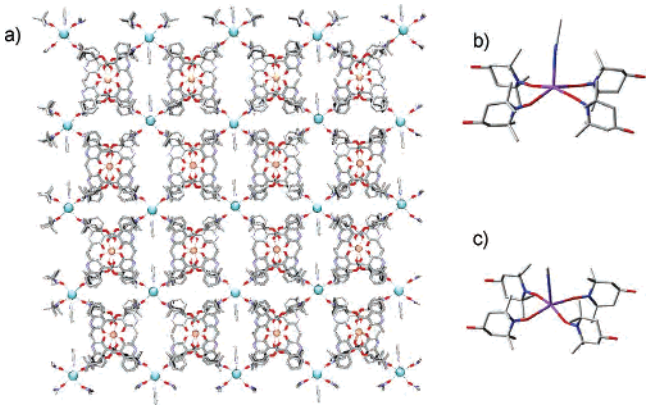


**Figure 2.** (a) Supramolecular 2D assembling of the $[Y(QT)_4]^-$ units by ionic bridges, with $\{K^+(QT)_4\}$ quasi-planar nodes. (b) The close view of the assembling nodes, $\{(CH_3CN)K^+(QT)_4\}$. (c) The idealization of the assembling nodes to the $C_{2v}$ symmetry.

**Table 1.** Crystallographic Data and Structural Refinement for $K[Y(QT)_4(CH_3CN)]\cdot 2CH_3CN\cdot {}^1/_4H_2O$

| empirical formula | $C_{86}H_{105.5}KN_{11}O_{16.25}Y$ |
|---|---|
| fw | 1681.32 |
| temp/K | 200(2) |
| $\lambda$/Å | 0.71073 |
| cryst syst | triclinic |
| space group | $P\bar{1}$ |
| $a$/Å | 15.3236(16) |
| $b$/Å | 15.4411(17) |
| $c$/Å | 21.331(3) |
| $\alpha$/deg | 111.181(3) |
| $\beta$/deg | 106.205(4) |
| $\gamma$/deg | 92.444(3) |
| $V$/Å$^3$ | 4460.9(9) |
| Z | 2 |
| $\rho_{calc}$/g cm$^{-3}$ | 1.252 |
| $\mu$ mm$^{-1}$ | 0.769 |
| $F$(000) | 1773 |
| cryst size/mm$^3$ | 0.45 × 0.30 × 0.25 |
| theta range for data collection/deg | 1.43−27.56 |
| index ranges | $-19 \le h \le 19$, $-20 \le k \le 20$, $-27 \le l \le 27$ |
| reflns collected | 44457 |
| independent reflns | 20327 [$R$(int) = 0.0612] |
| completeness to theta = 27.56° | 98.6% |
| refinement method | full-matrix least-squares on $F^2$ |
| data/restraints/params | 20327/0/1015 |
| GOF on $F^2$ | 0.840 |
| $R_1$, $wR_2$ ($I > 2\sigma(I)$) | 0.0575, 0.1363 |
| $R_1$, $wR_2$ (all data) | 0.1307, 0.1504 |
| largest diff peak and hole/e Å$^{-3}$ | 1.033 and −0.699 |

The oxygen donors of phenoxo type (O1, O5, O9, O13), that are bearing negative charges, show Y−O bonds ranging from 2.22 to 2.24 Å (see Table 2). The oxygen donors belonging to carbonyl type (O2, O6, O10, O14), show lower coordination strength, expressed in longer bonds, with Y−O between 2.39 and 2.49 Å. The bite angles of the chelates are about 68−70°, e.g., 69.56° for the O1−Y−O2 angle. The aperture of the nonchelatic O−Y−O angles oriented toward the same faces of the coordination polyhedron as the chelate ones, are about in the 73−76° range, e.g., the O1−Y−O14 is 73.66°. With respect to the depicted antiprism, the above-discussed angles are oriented toward upper or lower faces (see Figure 1a). Considering the angles between the upper and lower faces one may measure those between the chemically different donors of the two, upper and lower,

**Table 2.** Selected Bond Distances (Å) and Angles (deg) for the Complex $K[Y(QT)_4(MeCN)]\cdot 2MeCN\cdot {}^1/_4H_2O$[a]

| | | | |
|---|---|---|---|
| Y−O1 | 2.228(3) | Y−O2 | 2.388(3) |
| Y−O5 | 2.237(3) | Y−O6 | 2.473(3) |
| Y−O9 | 2.217(3) | Y−O10 | 2.491(3) |
| Y−O13 | 2.239(3) | Y−O14 | 2.439(3) |
| K−O4 | 2.663(3) | K−O8#2 | 2.659(3) |
| K−O12#3 | 2.699(3) | K−O16#1 | 2.612(3) |
| K−N9 | 2.761(8) | | |
| O4−N2 | 1.279(4) | O8−N4 | 1.283(4) |
| O12−N6 | 1.283(4) | O16−N8 | 1.282(4) |
| O1−Y−O2 | 69.56(9) | O1−Y−O5 | 149.42(9) |
| O1−Y−O6 | 82.77(9) | O1−Y−O9 | 83.15(10) |
| O1−Y−O10 | 132.71(9) | O1−Y−O13 | 109.14(10 ) |
| O1−Y−O14 | 73.66(9) | O2−Y−O5 | 89.38(9) |
| O2−Y−O6 | 69.24(9) | O2−Y−O9 | 135.33(9) |
| O2−Y−O10 | 154.31(9) | O2−Y−O13 | 76.13(9) |
| O2−Y−O14 | 116.35(9) | O5−Y−O6 | 68.78(9) |
| O5−Y−O9 | 98.34(10) | O5−Y−O10 | 74.11(9) |
| O5−Y−O13 | 85.74(9) | O5−Y−O14 | 136.83(9) |
| O6−Y−O9 | 72.89(9) | O6−Y−O10 | 120.07(9) |
| O6−Y−O13 | 136.52(9) | O6−Y−O14 | 150.72(9) |
| O9−Y−O10 | 67.92(9) | O9−Y−O13 | 147.98(9) |
| O9−Y−O14 | 87.04(9) | O10−Y−O13 | 83.00(9) |
| O10−Y−O14 | 68.45(9) | O13−Y−O14 | 69.38(9) |
| O4−K−O8#2 | 92.79(10) | O4−K−O12#3 | 85.30(9) |
| O4−K−O16#1 | 150.47(10) | O4−K−N9 | 91.19(18) |
| O8#2−K−O12#3 | 163.33(10) | O8#2−K−O16#1 | 83.46(10) |
| O8#2−K−N9 | 100.79(18) | O12#3−K−O16#1 | 90.05(10) |
| O12#3−K−N9 | 95.82(17) | O16#1−K−N9 | 118.31(18 ) |

[a] Symmetry codes: #1 $x-1, y, z$; #2 $-x+1, -y, -z$; #3 $-x+1, -y, -z+1$; #4 $x+1, y+1, z$.

ligands (e.g., O1−Y−O6, O9−Y−O14). Such angles are ranging between values of 83° and 89°. The selected angles sketch the measures of an elongated antiprism, with a relatively narrow distribution of bond lengths and angles along related series, supporting the idea of the approximate $D_2$ symmetry.

The contacts of supramolecular bridging (see Figure 2a) are measured by the K···O distances that range between 2.61 and 2.69 Å. The apical acetonitrile molecule (see Figure 2b) is semicoordinated, with a K···N distance of 2.76 Å. The polygonal surrounding of the potassium ion with oxygen atoms from the TEMPO groups is approximately a rectangle, with the smaller O−K−O angles of 83.4° and 85.6°, while larger ones are 90° and 92.8°. The quasi-rectangular $\{O_4\}$ has the 3.51 and 3.63 Å O···O short edges and 3.76 and 3.86 Å long ones. The coordinated acetonitrile molecule is roughly perpendicular to this approximate square, various O−K−N angles running between values of 90° and 118°. In this way, the coordination of the potassium ion as a supramolecular node is approximately square pyramidal. The pyramid formed by the K and O atoms is very flat, with the trans O−K−O angles 150.5° and 160.3°. The atoms of the triangular $\{C_2NO\}$ moiety are located almost in the same plane, with respect of a given ligand. Such averaged planes are oriented closely perpendicular to the $\{O_4\}$ approximate plane made of coordinating nitroxide groups. The deviation from perpendicularity is about 1−2°, indebting the further $C_{2v}$ idealization.

**Magnetic Susceptibility (Part I).** The magnetic susceptibility data show antiferromagnetic behavior. The clue of interpretation stays in the reasonable assumption that the exchange interactions are localized in the $[(CH_3CN)K^+(QT)_4]$ unit of the supramolecular structure, since potassium ion directly contacts the spin carriers of the system and the distance from another potassium ion is about 15.1 Å. Exchange interactions between radicals of the same $[Y(QT)_4]^-$ unit can be neglected due to the far distance from the central yttrium(III) metal ion (8.6 Å) and the long skeleton of $\sigma$ bonds interposed between the coordinating and radical parts of the QT ligands.

**Scheme 1** Topology of the Interactions Defining the Supramolecular Contacts and the Corresponding Spin Hamiltonian Parameters

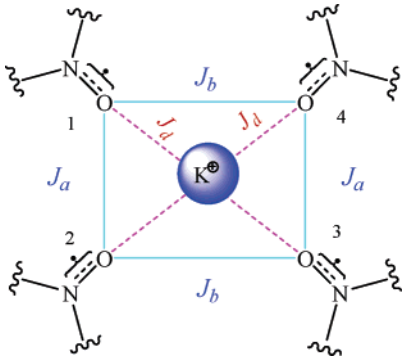


Considering the rectangular topology, the Heisenberg−Dirac van Vleck (HDVV) Hamiltonian for the system is

$$\hat{H}_{HDVV} = -2J_a(\hat{S}_1\cdot\hat{S}_2 + \hat{S}_3\cdot\hat{S}_4) - 2J_b(\hat{S}_2\cdot\hat{S}_3 + \hat{S}_4\cdot\hat{S}_1) - 2J_d(\hat{S}_1\cdot\hat{S}_3 + \hat{S}_2\cdot\hat{S}_4) \quad (1)$$

Here, $J_a$ and $J_b$ indicate the exchange parameters for coupling along the edges of the rectangle and $J_d$ for diagonal interaction (Scheme 1).

The system of four $^1/_2$ spins gives rise to the following set of states:

two singlets, $S = 0$, with the HDVV energies

$$E_{S_1} = J_a + J_b + J_d - 2\sqrt{J_a^2 + J_b^2 + J_d^2 - J_aJ_b - J_aJ_d - J_bJ_d} \quad (2a)$$

$$E_{S_2} = J_a + J_b + J_d + 2\sqrt{J_a^2 + J_b^2 + J_d^2 - J_aJ_b - J_aJ_d - J_bJ_d} \quad (2b)$$

three triplets, $S = 1$,

$$E_{T_1} = +J_a + J_b - J_d \quad (2c)$$

$$E_{T_2} = +J_a - J_b + J_d \quad (2d)$$

$$E_{T_3} = -J_a + J_b + J_d \quad (2e)$$

and one quintet, $S = 2$,

$$E_Q = -J_a - J_b - J_d \quad (2f)$$

The fit of the independent exchange parameters with respect to the experimental magnetic susceptibility data leads to the surprising tendency of equal $J$ parameters: $J_a \cong J_b \cong J_d \cong -3.93$ cm$^{-1}$ and $g = 2.039$. This result induced a challenging question regarding how this situation can be

achieved in the described system. At one hand, a reasonable assumption for the equality of $J$ parameters can apparently be found. Namely, if the potassium cation mediates the exchange via s-type orbitals, then the interactions can be considered insensitive to the mutual angular positions of the spins. In this case, the antiferromagnetic coupling can be thought the same for both cis and trans pairs of radicals, resulting in the obtained coincidence of the $J$ parameters. In this conjuncture, even with the rectangular topology, the spin system effectively behaves tetrahedral-like, yielding close degeneracy within the sets of the two singlets ($S = 0$) and the three triplets ($S = 1$) states.

On the other hand, a more critical approach can inquire this result as artifact due to parametric uncertainties. The pattern of antiferromagnetic susceptibility is obtained due to progressive population, at growing temperatures, of the triplet and quintet states starting from the singlet ground state. Considering that the susceptibility is a global thermodynamic data, a series of relatively close triplet states and a set of degenerate ones placed in the barycenter of the split set may show the same trend in $\chi T$ versus $T$. In the van Vleck susceptibility formula this approximation is held in the first order of the series expansion of energies with respect to a given barycenter. We decided therefore to investigate more deeply this phenomenon, by means of the ab initio calculations.

**Theoretical Analysis.** The GAMESS[43] package was used to perform the ab initio calculations within the CASSCF method. The computed system is the idealized $C_{2v}$ model, {(HCN)$K^+$(TEMPOL)$_4$}, closely resembling the {($CH_3CN$)-$K^+$(QT)$_4$} parts of the supramolecular structure. For the actual purpose the quinolinoyloxy moiety of the QT was replaced with a terminal OH group, using then the ligand known as TEMPOL (4-hydroxy-2,2,6,6-tetramethylpiperidine-*N*-oxyl) as a model of the interacting radicals. The 6-311G* basis set was used for the K, N, and O atoms and 6-31G for the remaining skeleton of the C and H atoms. The graphical illustration of the computation results were made with the help of the MOLEKEL utilities.[44]

We performed the CASSCF calculations within reduced, CASSCF(4,4), and enlarged, CASSCF(12,8), active spaces, where the ($n$, $m$) pairs denote the number of active electrons and active orbitals, respectively. The CASSCF(4,4) is based on the four orbitals, originating from the symmetry-adapted SOMO states of each TEMPOL fragment. Assigning the local $z$ axes along the NO bonds and the $x$ axes perpendicularly to the mean plane of the six-membered rings, the magnetic orbitals can be roughly described as $|\pi_{\perp}^{*}\rangle \approx N_1(p_x^{O} - p_x^{N})$. The extended active space of the CASSCF(12,8) calculation was built taking the next lower MOs from the canonical set of the first CASSCF(4,4) result. These MO have the appearance of rotating of 90° the above orbitals so that the antibonding MOs parallel to the reference plane are formed: $|\pi_{||}^{*-\mathrm{hyper}}\rangle \approx N_2(p_y^{O} - p_y^{N})$. Their designation as $\pi$ is formal, in the sense of hyperconjugation relationship. Namely, a lone pair on the oxygen interacts with a symmetry combination of parallel $\sigma$(C−N) bonds.

**Table 3.** Energy Levels from CASSCF Calculations and the HDVV Energies with the Fitted Parameters from the Section Magnetic Susceptibility (Part II)

| $S$ | label | symmetry | CASSCF(4,4) $E(^{2S+1}\Gamma_i)$ (cm$^{-1}$) | CASSCF(12,8) $E(^{2S+1}\Gamma_i)$ (cm$^{-1}$) | exp $E_{\mathrm{HDVV}}$ (cm$^{-1}$) |
|---|---|---|---|---|---|
| 0 | $S_1$ | $^1A_1$ | 0 | 0 | 0 |
| 1 | $T_1$ | $^3A_2$ | 4.776 | 8.611 | 9.053 |
| 1 | $T_2$ | $^3B_2$ | 8.299 | 15.342 | 15.871 |
| 0 | $S_2$ | $^1A_1$ | 9.405 | 16.945 | 18.106 |
| 1 | $T_3$ | $^3B_1$ | 10.122 | 18.136 | 19.325 |
| 2 | $Q$ | $^5A_1$ | 13.798 | 25.154 | 26.143 |

The CASSCF produces more states than those of the HDVV spin Hamiltonian (e.g., the CASSCF(12,8) implies 336 states with $S = 0$, asides of 378 states with $S = 1$ and 70 states with $S = 2$). The levels matching the HDVV states are undoubtedly identified as the lowest set with the corresponding spin multiplicities.

The relative energies from the CASSCF calculations are presented in Table 3. These sets can be fitted with respect to the corresponding gaps (a relative error of $\sim 10^{-4}$) equated by the formulas 2a−f. The CASSCF(4,4) reduced calculation is fitted with the following set of exchange parameters: $J_a = -2.710$, $J_b = -1.799$, $J_d = -0.039$ cm$^{-1}$. The extended CASSCF(12,8) version gives larger magnitudes: $J_a = -4.833$, $J_b = -3.436$, $J_d = -0.073$ cm$^{-1}$. Directly replaced in the van Vleck equation of the magnetic susceptibility, the first set underestimates the antiferromagnetism, showing the $\chi T$ slope at lower temperatures than the experimental data, while the second computed set practically matches the experimental curve.

For the interpretation insight, we looked beyond the visible excellent performance of the extended CASSCF(12,8) calculation. The numerical experiment of reduced and enlarged active spaces evidence that the ab initio calculations are well accounting for a given mechanism of interaction, even when the quantitative performance is not perfect. Indeed, the gaps and coupling constants are almost 2 times smaller in the reduced CASSCF, but the relative ordering of singlet, triplet, and quintet states, as well as the ratio of $J_a/J_b \approx 1.5$ while $J_d \approx 0$, is a stable result in both calculations. The improvements due to the larger active space are subtle. For a given state, the main contributing configurations are closely similar in the coefficients, in both the CASSCF(4,4) and CASSCF-(12,8) results. The extended calculation accounts better for the correlation energy on the expense of many higher excitations appearing with small coefficients. Also the canonical MOs carrying the spins are practically identical in both cases. Their graphical representations (the $|\pi_{\perp}^{*}\rangle$ from CASSCF(12,8) against those of CASSCF(4,4)) are in fact indistinguishable.

The spin population analysis, or the contour maps of the orbital and spin density (Figures 3 and 4), show almost equal spin distribution over the nitrogen and oxygen atoms. The Mulliken spin density corresponding to the computed

(43) Schmidt, M. W.; Baldridge, K. K.; Boatz, J. A.; Elbert, S. T.; Gordon, M. S.; Jensen, J. H.; Koseki, S.; Matsunaga, N.; Nguyen, K. A.; Su, S. J.; Windus, T. L.; Dupuis, M.; Montgomery, J. A. *J. Comput. Chem.* **1993**, *14*, 1347−1363.

(44) (a) Flukiger, P.; Luthi, H. P.; Portmann, S.; Weber, J. *MOLEKEL* 4.3; Swiss Center for Scientific Computing: Manno, Switzerland, 2000−2002. (b) Portmann, S.; Luthi, H. P. *Chimia* **2000**, *54*, 766−770.

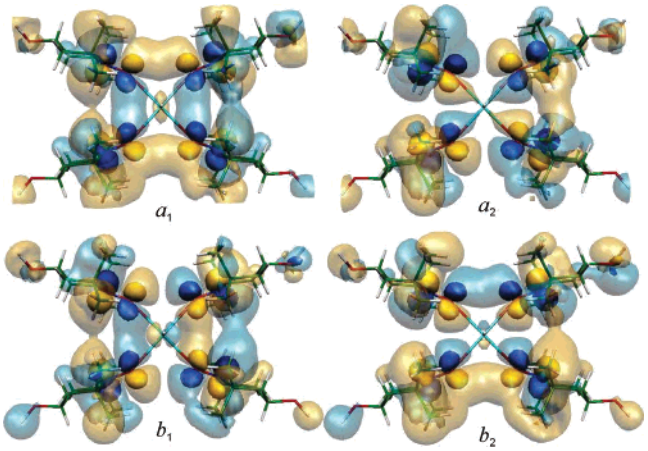


**Figure 3.** Canonical CASSCF orbitals and their symmetry labels in the $C_{2v}$ idealized geometry of {(HCN)$K^+$(TEMPOL)$_4$}. The transparent isosurfaces are drawn at 0.005 $e$/Å$^3$, the inner solid surfaces at 0.04 $e$/Å$^3$.

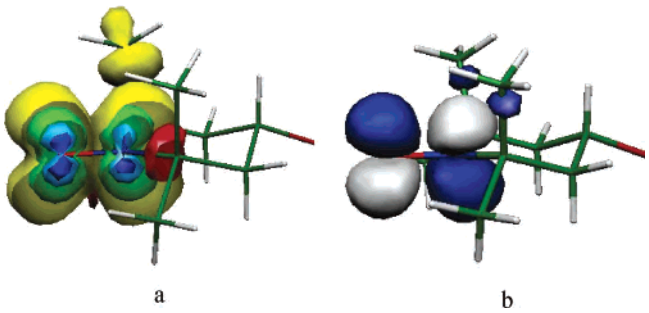


**Figure 4.** (a) Contour maps of the spin density from unrestricted DFT calculation on the free ligand QT (only the significant TEMPO moiety is included in the drawing). The successive contours, from inside to outside, correspond, respectively, to 0.1, 0.05, 0.025, and 0.005 electrons α/Å$^3$. The partial contour marked on the carbon side of the C−N bond (in red) corresponds to a slight spin polarization drawn at 0.005 $\beta$/Å$^3$. (b) The SOMO from restricted DFT calculation, ($\pi$-antibonding, at 0.01 $e$/Å$^3$ isosurface) on the free QT ligand.

CASSCF orbitals is 0.457 on oxygen and 0.492 on nitrogen. For the sake of comparison, the unrestricted DFT calculations were done for the same complex with the ADF[45] code using the TZP basis set and gradient-corrected Becke−Perdew functional. The spin populations with the ADF-DFT method are similar to the CASSCF ones, 0.433 on oxygen and 0.501 on nitrogen. The equal distribution of the spins over the N and O atoms is in line with experimental data from polarized neutron diffraction[8] corroborated also with related DFT calculations.[4]

The unrestricted DFT afforded information about spin polarization factors. The potassium ion shows a very small, 0.002α, spin population, with the same polarization as the radicals, while the carbon atoms near the nitrogen in the cycle show a slightly opposite polarization with 0.012$\beta$ spin. Therefore, no spin polarization phenomena are acting along the O···$K^+$···O path, and the polarization effects in the immediate organic skeleton are less important for the exchange coupling. An attempt to use the ADF methodology (enabling the input control of the spins on the fragments), in order to approach the broken symmetry estimation of the exchange effects, leads to a rather large overestimation of the coupling strength. Due to rather intricate methodology aspects, this problem will not be expanded here.

A glance at the computed CASSCF MOs (Figure 3) suggests the role of direct overlapping between the p AOs of the oxygen, tangentially oriented to the molecular rectangle. At low-valued contours the overlap density is evidenced along the edges. One may clearly see then why the exchange interaction is rather strongly distance dependent. The highest magnitude occurs along the shorter edge. In the $b_1$ and $b_2$ symmetries one may note the slight involvement of $p_x$ and $p_y$ orbitals on the potassium ion. The elliptic shape of the central density in the $a_1$ MO suggests the role of s and d AOs on the potassium. The small d implication is also visible in the slight deformation toward center of the low-density lobes at the $a_2$ symmetry component.

**Magnetic Susceptibility (Part II).** After the above conclusions we revised the HDVV account of the experimental magnetic susceptibility. The critical perspective is that in systems having a relative parametric complexity the automatic use of the best fit, when several other acceptable solutions are appearing, may be a trap that can be avoided with methodological carefulness.

With the outlined ab initio results, the possibility of equal exchange parameters is ruled out. Particularly, the parameter over the diagonal of the rectangle is negligible and the parameter over the short edge has the largest absolute value. As a criterion to validate the computed exchange parameters we also considered perfect fit of the ab initio energy gaps, with respect to the HDVV model.

Consequently, we made an alternate fitting, imposing $J_d = 0$. Even in this case, the tendency to obtain equal parameters persists, yielding $g = 2.010$, $J_a \cong J_b - 4.38$ cm$^{-1}$. Then we proceeded imposing the ratio, $J_a/J_b \cong 1.5$ as suggested by the calculations. The fit gives $g = 2.008$, $J_a = -5.14$ cm$^{-1}$, and $J_b \cong -3.41$ cm$^{-1}$, namely, a set with magnitudes remarkably close, quantitatively, to the CASSCF-(12,8) ab initio results. We incline to take this estimation as the reasonable interpretation of the experimental data, in the frame of the exposed reasons (Figure 5).

The absolute fit errors, taken as $R = (\sum_{i=1}^{N}((\chi T)_i^{exp} - (\chi T)_i^{fit})^2)^{1/2}/N$ (where $N$ is the number of recorded points) are 0.0043, 0.0056, 0.0059 cm$^3$ mol$^{-1}$ K, respectively, for the presented cases with $J_a = J_b = J_d$ versus $J_a = J_b$, $J_d = 0$ versus $J_a \neq J_b$, $J_d = 0$. Even though the absolute deviation may suggest the discarded alternatives, the outlined discussion clearly pointed the reasons for selection of the last set.

Figure 6 shows the results of the fitting $J_d$, (parameter value in Figure 6a and error $R$ in Figure 6b) when $J_a$ and $J_b$ are tuned in the range of −6 to 0 cm$^{-1}$. The point corresponding to the absolute minimum is marked by a circle in both maps. In Figure 6a one may visually intercept this point at the crossing near the ($J_a$, $J_b$, $J_d$) ∼ (−4, −4, −4) cm$^{-1}$ tick marks. The $J_d = 0$ plane is marked in gray in

(45) (a) ADF2004.01, SCM, Theoretical Chemistry, Vrije Universiteit, Amsterdam, The Netherlands, http://www.scm.com. (b) Fonseca, Guerra, C.; Snijders, J. G.; te Velde, G.; Baerends, E. J. *Theor. Chem. Acc.* **1998**, *99*, 391−403. (c) te Velde, G.; Bickelhaupt, F. M.; van Gisbergen, S. J. A.; Fonseca, Guerra, C.; Baerends, E. J.; Snijders, J. G.; Ziegler, T. *J. Comput. Chem.* **2001**, *22*, 931−967.

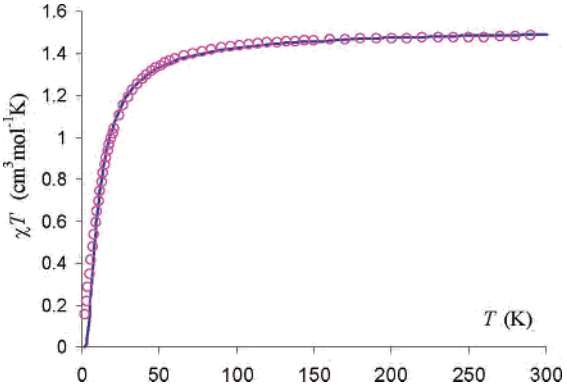


**Figure 5.** Magnetic susceptibility data, $\chi T$ vs $T$ (experiment = circles, model = continuous line)

Figure 6a. The minimum constrained to $J_d = 0$, denoted by a triangle, is obtained in the $J_a = J_b$ symmetry point. The point selected by the above-discussed critical approach, is marked with asterisk in Figure 6, parts a and b. The ab initio analysis showed that the parameters should obey the $|J_a| > |J_b|$ and $J_d \sim 0$ relationship and there are no reasons for higher pseudosymmetrical parametric regularities, as, on the other hand, the direct fitting suggests. The full parametric mapping illustrates an important caveat on the artifacts possible in the brute fitting of experimental data and the valuable help of the theoretical counterpart. Details are presented in the Supporting Information.

**Dipolar Coupling and EPR Spectra.** EPR spectroscopy is a powerful technique which allows a deeper investigation of the interactions in radical systems.[19,46] The EPR details of the actual system are governed by the dipolar coupling between the NO radical groups, the rationalization being in line with the above-discussed rectangular topology.

The macroscopic form of the dipolar interaction (in SI units) is described by the following equation:

$$E_{AB} = \frac{1}{4\pi\epsilon c^2}\left(\frac{\boldsymbol{\mu}_A\cdot\boldsymbol{\mu}_B}{r_{AB}^{\ 3}} - 3\,\frac{(\boldsymbol{\mu}_A\cdot\mathbf{r}_{AB})(\boldsymbol{\mu}_B\cdot\mathbf{r}_{AB})}{r_{AB}^{\ 5}}\right) \tag{3}$$

where the $\boldsymbol{\mu}_A$, $\boldsymbol{\mu}_B$ symbols refer to the vector quantities of the interacting magnetic dipole moments, $\mathbf{r}_{AB}$ and $r_{AB}$, defining the vector and distance between their mutual position in the space points $A$ and $B$. Replacing the quantum definitions of the moment ($\boldsymbol{\mu} = g\mu_B\hat{S}$) the dipolar interaction is put in the tensor form:

$$\hat{H}_{\mathrm{dip}}^{AB} = \hat{S}_A\cdot\mathbf{D}_{AB}\cdot\hat{S}_B = \hat{S}_B\cdot\mathbf{D}_{AB}\cdot\hat{S}_A = \sum_{\xi=x,y,z}\sum_{\zeta=x,y,z} D_{AB}^{\xi\xi}\,(\hat{S}_A^{(\xi)}\hat{S}_B^{(\zeta)}) \tag{4}$$

with tensor elements

$$D_{AB}^{\xi\xi} = D_{AB}(1 - \delta_{\xi\zeta}/3)(\lambda_{AB}^{(\zeta)}\lambda_{AB}^{(\xi)}) \tag{5}$$

expressed with respect to the directory cosines $\lambda_{AB}^{(\zeta)} = \mathbf{r}_{AB}^{(\zeta)}/|r_{AB}|$ and the dipolar magnitude

$$D_{AB} = -3\cdot\frac{g^2\mu_B^{\ 2}}{4\pi\epsilon c^2}\left\langle\frac{1}{r_{AB}^{\ 3}}\right\rangle \tag{6}$$

The angular bracket $\langle 1/r_{AB}^3\rangle$ in the definition of the $D_{AB}$ dipolar magnitude parameter denotes the expectation value integrated over the localized spin distributions. In well-separated systems the simple use of the $1/r_{AB}^3$ geometrical distance can be made. The details of the Hamiltonian derivation are given in the Supporting Information. The total dipolar Hamiltonian that constitutes the source of zero-field splitting (ZFS) effects on the collective spin states is obtained summing over all the pairs of interacting spins.

$$\hat{H}_{\mathrm{dip}}^{AB} = \sum_{A-1B<A}^{4}\sum\hat{H}_{\mathrm{dip}}^{AB} \tag{7}$$

The labeling of the $D_{AB}$ parameters is parallel to those assigned to the $J_{AB}$ in Scheme 1. Namely, the designation is $D_a$ for the 1−2 and 3−4 edges, $D_b$ for the 2−3 and 1−4 ones, while $D_d$ over the diagonals. Applying the above Hamiltonian to the triplet states and keeping their labeling as adopted in the HDVV section, the energies are expressed with the help of general ZFS operators added to the HDVV Hamiltonian blocks:

$$\bar{E}_{\mathrm{T}_i} = E_{\mathrm{T}_i} + D_i\left(S_{z_i}^{\ 2} - \frac{1}{3}\hat{S}_i^{\,2}\right) + E_i(S_{x_i}^{\ 2} - S_{y_i}^{\ 2}) \tag{8}$$

The formal ZFS components for each triplet, with the label 1 corresponding to the lowest one, are

$$D_1 = D(T_1) = \frac{1}{4}(-D_a - D_b + D_d);$$

$$E_1 = E(T_1) = \frac{1}{4}(D_a - D_b) \tag{9a}$$

$$D_2 = D(T_2) = \frac{1}{4}(-D_a + D_b - D_d);$$

$$E_2 = E(T_2) = \frac{1}{4}(D_a + D_b) \tag{9b}$$

$$D_3 = D(T_3) = \frac{1}{4}(D_a - D_b - D_d);$$

$$E_3 = E(T_3) = \frac{1}{4}(D_a + D_b) \tag{9c}$$

We confine to this point our Hamiltonian component analysis, mentioning that further details and results will be the object of another work.

The exchange-coupled nature of the system is reflected in the aspect of the EPR signal at the recorded temperatures. At 10 K the EPR spectrum is rich in details as shown in Figure 7. The resonance absorption shows a central signal with pairs of shoulders, symmetrically placed to the central field, $H_0$. These shoulders are emerging toward attenuation with increasing temperatures. The pattern can be tentatively explained in terms of dipolar interactions in the rectangle of four interacting radicals.

(46) Ziessel, R.; Stroh, C.; Heise, H.; Köhler, F. H.; Turek, P.; Claiser, N.; Souhassou, M.; Lecomte, C. *J. Am. Chem. Soc.* **2004**, *126*, 12604−12613.

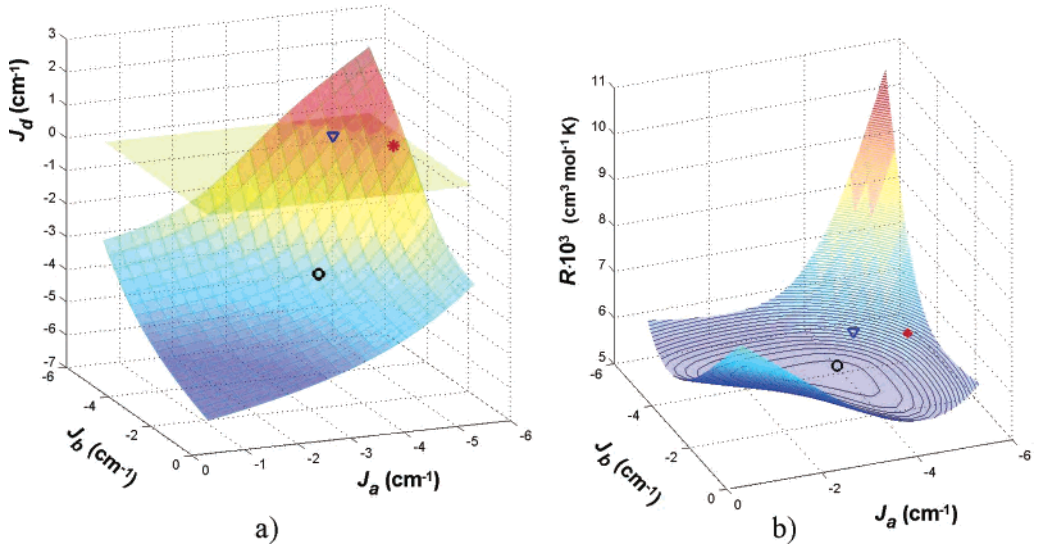


**Figure 6.** Results of the full parametric fit with respect to the experimental $\chi T$ data: the fitted $J_d$ parameter (a) and the error map (b) when $J_a$ and $J_b$ are varied in the depicted range. The circle (○) marks the point corresponding to the absolute minimum, the triangle (▽) the constrained minimum at $J_d = 0$, and the red asterisk (∗) the point selected according to the supplementary outlined physical criteria.

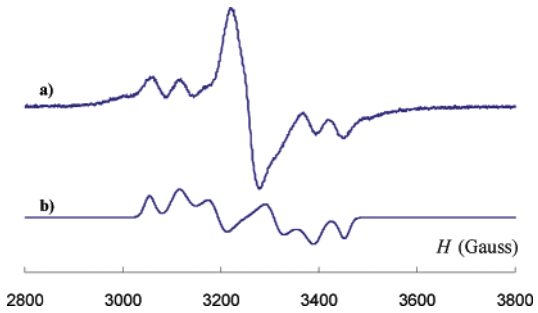


**Figure 7.** (a) EPR spectrum obtained at 10 K and (b) the simulated spectrum of the lowest triplet state, with the parameters of $D = 198$ G and $E = 26.8$ G.

Using ZFS parameters $D_1 = 198$ and $E_1 = 26.8$ G, we simulated the lowest triplet obtaining a remarkable matching with the pair shoulders.

The four spins can be considered as placed in the middle of the NO bonds, being separated by the following distances, $R_a = 4.30$, $R_b = 4.70$, $R_d = 6.37$ Å. Applying the dipolar estimation, one obtains $D_a = -700.4$, $D_b = -535.9$, $D_d = -215.3$ G. Replacing the parameters in eq 9a the ZFS parameters for the lowest triplet are $|D_1| = \sim 250$, $|E_1| = \sim 40$ G, in reasonable agreement with the fitted parameters describing the shoulders of the experimental spectrum.

Several attempts of improving the fit global fit lead toward intriguing versions, pointing toward the breakdown of parallelism with the dipolar approximation. Being aware of possible numerical artifacts of local nonunique solutions, in the frame of rather large parametric degree of freedom of the case, we decline ourselves the tractability of the complete analysis of this problem. Presumably, complex kinetic mechanisms of spin−spin and spin−lattice relaxations are acting, driving the line profile and temperature dependence. We qualitatively assume that the central line in the present experiments is mainly due to a portion of the system that behaves as having effectively reached the paramagnetic limit, due to rapid processes, occurring among the excited states and contributing with an apparently quasi-isotropic signal over the part of the spectrum that still bears details of the lowest triplet state resolution of the splitting. Indeed, after 30 K the EPR spectrum becomes a broad isotropic line.

Detailed new experiments on single crystals and at lower temperatures are in progress, aiming to solve the open questions in a future related work dedicated to the specialized EPR analysis. We conclude the present work in the general frame of the presented interdisciplinary approach that consistently addressed molecular, supramolecular, electronic, and magneto−structural paradigms.

## Conclusions

The crystals structure of a new tetra(quinoline−TEMPO)-yttrium potassium salt complex has been presented, showing a supramolecular assembly through coordination of the TEMPO free radicals to the potassium counterion. The magnetic properties originating from the rectangular system of four interacting nitroxides have been analyzed by the measurement of magnetic susceptibility. The ab initio CASSCF calculations provided an appropriate interpretation of the antiferromagnetic behavior and elucidated the mechanism of interactions within the complex. Observing that the automatic fit of spin coupling constants to the experimental susceptibility leads to pseudosymmetry parametrical relationships that are clearly discarded by the critical ab initio analysis, a methodological caveat is raised in this respect. Taking the case as a prototype study we illustrated the complementary use of the ab initio approach to decide the reasonable phenomenology. The EPR measurement at 10 K provided a closer look at the system, and the simulated spectrum in the lowest excited triplet state has been presented. This complex is potentially the first of a new series of molecules of this kind. By substitution of the central diamagnetic yttrium metal ion with paramagnetic one new interesting magnetic properties can be expected and interpreted by subtraction of the results presented here.

**Acknowledgment.** This work was supported by a Grant-in-Aid for Scientific Researchers No. 165500031 from the Ministry of Education, Science, Culture and Sports, Japan. M.F. thanks the JSPS (P04390) and CNCSIS/RO (2005/886) for financial support. F.C. acknowledges the COE support for the fellowship in Tohoku University and CNCSIS/RO (2005/1422).

**Supporting Information Available:** X-ray crystallographic data in CIF format, supplementary details about the magnetic susceptibility fit, ab initio calculations, and the dipolar spin coupling Hamiltonian. This material is available free of charge via the Internet at http://pubs.acs.org.

IC0610841